Check for updates

ChemPhotoChem

Research Article
doi.org/10.1002/cptc.202500039

Chemistry Europe
European Chemical Societies Publishing

www.chemphotochem.org

Red-to-Near-Infrared Electroluminescence and Low-Threshold Amplified Spontaneous Emission from Solution-Processable Fluorescent Diketopyrrolopyrrole Derivatives

Anthony D' Aléo,* Virginie Placide, Hao Ye, Matteo Fornasarig, Danillo Valverde, Eunyoung Choi, Gabriel Canard, Jeong Weon Wu, Yoann Olivier,* Chihaya Adachi,* and Jean-Charles Ribierre*

A detailed investigation of the photophysical, electroluminescence, and amplified spontaneous emission (ASE) properties of two solution-processable fluorescent diketopyrrolopyrrole derivatives is reported. Photophysical measurements are carried out in solution and blend films containing a 4,4′-bis(*N*-carbazolyl)-1,10-biphenyl (CBP) or a poly[(9,9-di-*n*-octylfluorenyl-2,7-diyl)-alt-(benzo[2,1,3] thiadiazol-4,8-diyl)] host, to gain important insights into the excited state behavior of these dyes. Quantum chemical calculations are also carried out to support the experimental findings. An optimization of the doping concentration in the CBP blends is necessary to reduce the strong aggregation. This optimization led for both near-infrared-emitting dyes to a substantial increase of the photoluminescence quantum yield, which can reach values as high as 60%. It is also found that the blend films show excellent ASE properties with a threshold as low as 3.5–4.5 μJ cm^{-2} for peak wavelengths of 739 and 727 nm. In addition, the electroluminescence properties of the two organic laser dyes are examined in organic light-emitting diodes (OLEDs). The best OLED device shows a maximum external quantum efficiency value of around 2%. Overall, this study demonstrates the excellent potential of diketopyrrolopyrrole derivatives for high-performance near-infrared organic semiconductor lasers and provides useful information for the design of new efficient near-infrared emitters for optoelectronic applications.

1. Introduction

Intensive research effort has recently focused on low-energy bandgap materials for applications in organic solar cells,[1–4] organic field-effect transistors (OFET),[5–9] and organic light-emitting diodes (OLEDs).[10–14] In particular, a wide variety of light-emitting compounds have been developed to achieve efficient far-red and near-infrared (NIR) OLEDs, including fluorescent small molecules and conjugated polymers,[15–19] phosphorescent heavy metal complexes,[20–22] and lanthanides complexes.[23,24] Although the photoluminescence quantum yield (PLQY) of these organic light-emitting materials is generally lower in the NIR region than for emitters in the visible, which is related to the so-called energy-gap law,[25] phosphorescent platinum complexes have been used in highly efficient NIR OLEDs with external quantum efficiency (EQE) exceeding 20%.[26–29] Another approach to producing OLEDs with 100% internal quantum efficiency is based on the use of thermally activated delayed fluorescence

A. D' Aléo
Institut de Physique et Chimie des Matériaux de Strasbourg (IPCMS)
UMR 7504
CNRS-Université de Strasbourg
23 Rue du Loess, 67034 Strasbourg Cedex 2, France
E-mail: anthony.daleo@ipcms.unistra.fr

V. Placide, E. Choi, J. W. Wu
Department of Physics
Ewha Womans University
Seoul 03760, South Korea

H. Ye, C. Adachi, J.-C. Ribierre
Center for Organic Photonics and Electronics Research (OPERA)
Kyushu University
Motooka 744, Nishi, Fukuoka 819-039, Japan
E-mail: adachi@opera.kyushu-u.ac.jp
jr43@st-andrews.ac.uk

M. Fornasarig, D. Valverde, Y. Olivier
Laboratory for Computational Modelling of Functional Materials
Namur Institute of Structured Matter
University of Namur
Rue de Bruxelles 61, 5000 Namur, Belgium
E-mail: yoann.olivier@unamur.be

G. Canard
Campus de Luminy
Aix Marseille Univ, CNRS, CINaM UMR 7325
Case 913, 13288 Marseille, France

C. Adachi, J.-C. Ribierre
Adachi Molecular Exciton Engineering Project
Japan Science and Technology Agency (JST)
ERATO
Fukuoka 819-0395, Japan

J.-C. Ribierre
Organic Semiconductor Centre, SUPA
School of Physics and Astronomy
University of St Andrews
North Haugh, Fife KY16 9SS, UK

Supporting information for this article is available on the WWW under https://doi.org/10.1002/cptc.202500039

© 2025 The Author(s). ChemPhotoChem published by Wiley-VCH GmbH. This is an open access article under the terms of the Creative Commons Attribution License, which permits use, distribution and reproduction in any medium, provided the original work is properly cited.

© 2025 The Author(s). ChemPhotoChem published by Wiley-VCH GmbH

23670932, 2025, 7, Downloaded from https://chemistry-europe.onlinelibrary.wiley.com/doi/10.1002/cptc.202500039 by Ewha Womans University Library, Wiley Online Library on [07/12/2025]. See the Terms and Conditions (https://onlinelibrary.wiley.com/terms-and-conditions) on Wiley Online Library for rules of use; OA articles are governed by the applicable Creative Commons License

(TADF) emitters.[30] Curcuminoid borondifluoride[31–34] and multi-resonance emitters[35] are two families of dyes showing TADF properties that have been used in high-efficiency NIR OLEDs. Considering the potential applications of far-red/NIR OLEDs and organic semiconductor lasers in bioimaging, photodynamic therapy, sensors, information-secured displays, and optical telecommunication, further studies are still required to design and develop a next generation of more efficient NIR emitters for organic electroluminescent and/or lasing devices.

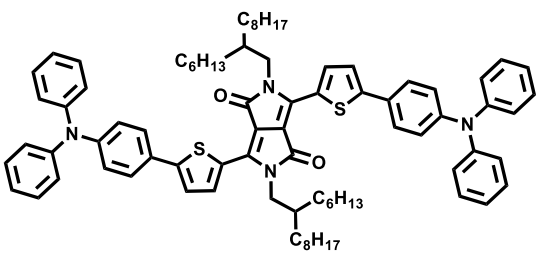
Among the variety of low bandgap materials developed for organic optoelectronics, there has been a growing interest in diketopyrrolopyrrole (DPP) derivatives, due to several advantages such as their strong optical absorption, easy and scalable synthesis, remarkable chemical and thermal stability, as well as the excellent PL properties of some of these dyes in the 700–800 nm spectral region when the DPP is conjugated with thiophene units.[36–38] Noticeably, these materials have been studied in solar cells, sensors, ambipolar field-effect transistors, and OLEDs.[39–45] Few reports have also suggested that DPP derivatives could be of interest for organic semiconductor lasers.[46,47] Despite these promising works, it should be, however, mentioned that most DPPs tend to strongly aggregate in solid-state due to π–π intermolecular interactions, which leads to a significant aggregation-caused quenching of their emission in thin films and has seriously limited their potential use in organic light-emitting devices so far.[48] In the present study, we have investigated the photophysical, electroluminescence (EL), and amplified spontaneous emission (ASE) properties of two donor–acceptor–donor (D–A–D) DPP derivatives where the thiophene units are capped by donor groups. The chemical structure of these two dyes is displayed in **Figure 1**.

The compound with the triphenylamine (TPA) moieties at both extremities of the DPP core (TPA–DPP–TPA) has already been synthesized and investigated in the context of organic solar cells[49,50] and photodynamic therapy.[51] This dye was also used in a more fundamental study aiming at improving the understanding of the structure–radical–property relationship of organic semiconductors.[52] Regarding the dye-containing carbazole (Cz) groups at both ends of the DPP core (Cz–DPP–Cz), the introduction of carbazole moieties into the molecular structure was motivated by its potential impact on the charge transport, photophysical properties, and the possibility of improving our understanding of the structure–properties relationships of this class of NIR-emitting laser dyes since such carbazole groups are less donating than TPA units. The results obtained with these two compounds provide clear evidence that advanced DPP derivatives with high PLQY in doped thin films and low ASE threshold are promising candidates for high-efficiency far-red/NIR solution-processed OLEDs and organic semiconductor lasers.

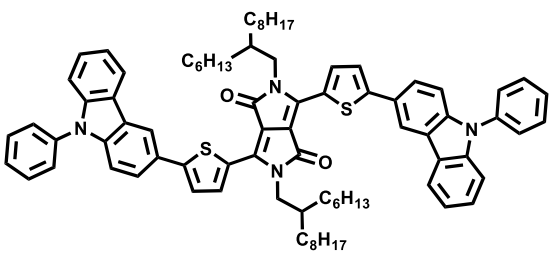
2. Results and Discussion

The synthesis of TPA–DPP–TPA and Cz–DPP–Cz (Figure S1, Supporting Information) and the characterization of their chemical properties are described in Figure S2–S5, Supporting Information. Starting from the commercially available 3,6-bis(5-bromothiophen-2-yl)-2,5-bis(2-hexyldecyl)-2,5-dihydropyrrolo[3,4-c]pyrrole-1,4-dione, Suzuki–Miyaura cross-coupling was performed using 4-(diphenylamino)phenylboronic acid and 9-phenylcarbazole-3-boronic acid to yield, respectively, TPA–DPP–TPA and Cz–DPP–Cz. The cyclic voltammetry of the two dyes is displayed in Figure S6, Supporting Information. The dyes present one-electron oxidation and reduction waves that can be associated with the donor units, including TPA, carbazole, and thiophene units, and the acceptor DPP core, respectively. The reduction potentials were measured to be identical at −1.67 V and −1.68 V (vs ferrocene/ferrocenium) indicating that the same DPP unit plays the role as acceptor. The first oxidation potentials were measured to be 0.20 V for TPA–DPP–TPA and 0.24 V for Cz–DPP–Cz, respectively (vs ferrocene/ferrocenium) implying that TPA–thiophene is a better donor than the carbazole–thiophene. The highest occupied molecular orbital (HOMO) and lowest unoccupied molecular orbital (LUMO) energies were then calculated using the oxidation and reduction potentials following the equation reported elsewhere.[12] This leads to HOMO and LUMO energies of −5.33 and −3.46 eV for TPA–DPP–TPA, respectively, which is in good agreement with the previously published data.[50] In the case of Cz–DPP–Cz, the HOMO and LUMO energies were found to be −5.37 and −3.45 eV, respectively.

The photophysical properties of TPA–DPP–TPA and Cz–DPP–Cz were examined at concentrations in the order of 1×10^{-6} M in solvents of different polarities. Their UV/vis absorption spectra, which are displayed in Figure S7a and S8a, Supporting Information, exhibit an intense structured band between 500 and 700 nm. The maximum absorption wavelengths of those dyes, which are listed in Table S1 and S2, Supporting Information, do not significantly shift with the polarity of the solvents. For the two



TPA-DPP-TPA



Cz-DPP-Cz

Figure 1. Chemical structures of the two investigated dyes.

© 2025 The Author(s). ChemPhotoChem published by Wiley-VCH GmbH

23670932, 2025, 7, Downloaded from https://chemistry-europe.onlinelibrary.wiley.com/doi/10.1002/cptc.202500039 by Ewha Womans University Library, Wiley Online Library on [07/12/2025]. See the Terms and Conditions (https://onlinelibrary.wiley.com/terms-and-conditions) on Wiley Online Library for rules of use; OA articles are governed by the applicable Creative Commons License

compounds, the low-energy absorption bands with a maximum ε value of around 82,000 M^{-1} cm^{-1} are assigned to a strongly allowed π–π* transition.[53] Such a high molar absorption coefficient is important to obtain high-gain materials. Furthermore, the fluorescence data of the two DPP derivatives in solution are summarized in Table S1 and S2, Supporting Information. As shown in Figure S7b and S8b, Supporting Information, their emissions lie in the far-red/NIR region. The steady-state PL spectra of TPA–DPP–TPA measured in the different solvents are more shifted toward a longer wavelength than those of Cz–DPP–Cz. This can be explained by the fact that TPA is a stronger donor than the phenylcarbazole moiety as evidenced above. Interestingly, the steady-state PL spectra of both dyes are not strongly affected by the solvent polarity. For instance, the maximum emission wavelength of TPA–DPP–TPA only varies from 652 nm in cyclohexane to 674 nm in acetonitrile while no clear trend can be observed in the case of Cz–DPP–Cz. Looking at Figure S7 and S8, Supporting Information, the observed behavior of the UV/vis absorption and fluorescence spectra as a function of the polarity of the solvents provides evidence that the ground state (S_0) and the first singlet excited state (S_1) of the two DPP derivatives are π–π* in nature. This statement is fully supported by the very small Stokes shift (See Figure S7 and S8, Table S1 and S2 and the Lippert–Mataga plot in Figure S9, Supporting Information) and the structuration of the steady-state PL spectra. PLQY and PL decays of the two dyes were then measured in the different solvents. As summarized in Table S1 and S2, Supporting Information, the PLQY does not significantly depend on the solvent polarity with values for TPA–DPP–TPA and Cz–DPP–Cz in the range 56–62% and 61–70%, respectively. The higher PLQY is measured for the Cz–DPP–Cz solution, which is in line with the energy-gap law since the emission is less redshifted compared to the ones of TPA–DPP–TPA. Furthermore, the measured PL decays of the two dyes in the solvents of different polarities were found to be monoexponential (Tables S1 and S2, Supporting Information) and do not show any delayed fluorescence in solution despite their D–A–D molecular architecture similar to the NIR curcuminoid derivatives recently used as emitters in highly efficient TADF OLEDs.[31] In accordance with the PLQY values, the PL lifetimes do not significantly vary with the polarity of the solvents and yields values around 2.3–2.6 ns and 2.6–2.9 ns for TPA–DPP–TPA and Cz–DPP–Cz, respectively. It is worth noting that the fluorescence radiative decay rates of TPA–DPP–TPA and Cz–DPP–Cz, calculated from the PLQY and PL lifetime values, are in the order of 2.5×10^8 s^{-1}. Such rates are in line with the strongly allowed transition resulting in fast fluorescence decays and the large oscillator strength well above 1 computed for the two compounds (Table S3, Supporting Information). Considering the importance of a high fluorescence radiative decay rate for achieving low ASE and lasing thresholds,[54–58] these results suggest that both dyes could be promising candidates for NIR organic semiconductor lasers.

Quantum chemical calculations were carried out to better understand and elucidate the ground (excited) state(s) properties of Cz–DPP–Cz and TPA–DPP–TPA molecules at the density functional theory level of theory with PBE0 and ωB97X-D functionals together with the 6-31G(d,p) basis set. The choice of these functionals allows to compare the results obtained with a global hybrid and a long-range corrected functional as well as to evaluate the effect of dispersion forces. Vibronically resolved emission and UV/vis absorption properties were also computed within the Franck–Condon approximation using the vertical hessian (VH) approach[59] (all computational details can be found in the Supporting Information). All derived photophysical properties and the vibronic-corrected absorption/emission spectra for the dyes are displayed in Table S3 and Figure S10, Supporting Information. We started by investigating the relative stability of the rotational isomers (rotamers) of the two compounds in the ground state. Figure S11, Supporting Information, presents the structures of the four rotational isomers of the thiophene–DPP–thiophene bonds optimized at the ωB97X-D/6-31G(d,p) level of theory, and their structural properties are summarized in Table S4, Supporting Information. The *trans–cis* isomer structure labeled (b) shows the same optical properties as its enantiomer *cis–trans*. The most stable isomer is the (c) *cis–cis*, where hydrogen bonding occurs between the oxygen atoms of the DPP core and the hydrogen atoms of the thiophenes. This configuration promotes the highest planarization of the thiophenes, and it was used for all the other calculations. Structures (a) *trans–trans* and (b) *trans–cis* are less stable by 7.6 and 17 kJ mol^{-1}, respectively, compared to structure (c) *cis–cis*. These less stable isomers exhibit one or both thiophene groups tilted by more than 20° for the S–O steric hindrance. Therefore, the *cis–cis* vertical absorption energy is redshifted with respect to the other two isomers. A Boltzmann population analysis reveals that 91.25% of the molecules adopt the (c) *cis–cis* conformation at 300 K, confirming it as the most relevant isomer. This is why our analysis will be only based on the *cis–cis* rotamer.

Our theoretical predictions agree with the experiments, which assign a π–π* transition for the S_1 state of both systems. This transition is predominantly dominated by a one-electron promotion from HOMO to LUMO orbitals (weight > 90%), exhibiting a locally excited character as suggested by the magnitude of the ϕ_S value (>0.85) characterizing the overlap between the hole and electron densities (see Figure S12, Supporting Information) as computed in the attachment–detachment formalism.[60] This local aspect is also confirmed by the visualization of the hole and electron density plots, showing that the electronic transition essentially involves the DPP core and the thiophene groups (see Figure S12, Supporting Information). The ωB97X-D functional predicts a slightly twisted ground state geometry (≈6° and 9° for the TPA–DPP–TPA and Cz–DPP–Cz, respectively), while calculations with the PBE0 functional result in a planar geometry. This suggests that dispersion forces induce a slightly twisted conformation TPA–DPP–TPA and Cz–DPP–Cz ground state optimized geometry. This feature could help to partially explain the larger S_1 excitation energy vertical excitation from the ground state (≈0.4 eV) predicted by the ωB97X-D functional with respect to the PBE0. The difference in the ground state geometry between the two functionals leads to a difference in larger reorganization and Stokes shift (see Table S7, Supporting Information).

As can be seen in Figure S10, Supporting Information, the vibronically simulated absorption spectrum at the PBE0/6-31G(d,p) level of theory has a strong absorption band for both dyes with peaks centered around 600 and 650 nm for

© 2025 The Author(s). ChemPhotoChem published by Wiley-VCH GmbH

23670932, 2025, 7, Downloaded from https://chemistry-europe.onlinelibrary.wiley.com/doi/10.1002/cptc.202500039 by Ewha Womans University Library, Wiley Online Library on [07/12/2025]. See the Terms and Conditions (https://onlinelibrary.wiley.com/terms-and-conditions) on Wiley Online Library for rules of use; OA articles are governed by the applicable Creative Commons License

Cz–DPA–Cz and TPA–DPP–TPA, respectively, in quite good agreement with the experiments. In addition, the emission spectrum displays a band ranging from 700 up to 750 nm, consistent with the experimental spectra in solution (Figure S10, Supporting Information) for Cz–DPA–Cz and TPA–DPP–TPA, respectively. The ωB97X-D/6-31G(d,p) method predicts similar absorption and emission spectra, although both are blueshifted compared to those predicted by PBE0. Both compounds bear an $S_0 \rightarrow S_1$ oscillator strength larger than 1 with both functionals, resulting in predicted fluorescence radiative decay rates in the range of $2.0–2.5 \times 10^8\ s^{-1}$ which are in good agreement with the experimental data (Tables S1 and S2, Supporting Information). The low Huang–Rhys factors for all positive harmonic vibrational normal modes support the validity of the calculations (Figure S13, Supporting Information). However, within the VH method, modes with imaginary frequencies were identified for the S_0 state in emission and for the S_1 in absorption. These modes, which primarily correspond to structural bendings of the dyes, were excluded from the vibrational space in all calculations (Figure S14, Supporting Information) as suggested in refs. [61,62]. In addition, these modes are highly anharmonic and cannot be accurately described within the harmonic approximation. However, their exclusion could contribute to the less structured emission and absorption computed spectra compared to experimental ones (Figure S7, S8 and S10, Supporting Information). Their contribution could be evaluated if an approach including anharmonic effects were considered, which is beyond the scope of this work. It is also important to note that these calculations were performed for isolated gas-phase molecules. Environmental effects, such as solvation, can influence absorption and fluorescence peak positions, band broadening, and vibrational mode coupling.[61,63]

To fabricate high-efficiency OLEDs and organic semiconductor lasers, concentration quenching of the fluorescence due to intermolecular interactions and aggregation in thin films needs to be suppressed. For this purpose, the DPP dyes were blended at different doping concentrations into a 4,4′-bis(*N*-carbazolyl)-1,10-biphenyl (CBP) host. In addition, since no delayed fluorescence was observed, the dyes were also blended in low-lying triplet excited state poly[(9,9-di-*n*-octylfluorenyl-2,7-diyl)-alt-(benzo[2,1,3]thiadiazol-4,8-diyl)] (F8BT) to estimate the PLQY in that environment. Those host materials were chosen based on their respective HOMO and LUMO energy values (Figure S15a, Supporting Information) and the spectral overlap between their fluorescence spectra and the absorption spectra of the DPP dyes (Figure S15b,c, Supporting Information). Such a blend configuration should promote an efficient Förster resonant energy transfer (FRET) of the singlet excitons from both host materials to the dopants while preventing a quenching of the emission by photoinduced electron transfer or exciplex formation. As shown in Figure S15b, Supporting Information, while FRET should take place from the CBP host to the $S_0–S_2$ of the DPP dopants, a more efficient FRET should take place from the CBP host to the $S_0–S_1$ of the DPP dopants (Figure S15c, Supporting Information).[64–66]

The absorption spectra of the CBP and F8BT blends at different doping concentrations varying from 1 to 6 wt% are displayed in **Figure 2** and S16, Supporting Information, for Cz–DPP–Cz and TPA–DPP–TPA, respectively. Due to the low concentrations of the DPP derivatives in these blends, these spectra are dominated by the absorption of the host molecules in the UV–vis region (296 and 326 nm for CBP and 319 and 454 nm for F8BT). As expected from the measurements in solution, the absorption due to the π–π* transition of the dyes can be observed between 550 and 650 nm (Figure 2 and S16, Supporting Information). As reported in Tables S5–S8, Supporting Information, the maximum absorption wavelengths of these low energy transitions do not change as a function of the doping concentration and are measured to be around 645 and 635 nm for TPA–DPP–TPA and Cz–DPP–Cz in CBP host and 643 and 635 nm for TPA–DPP–TPA and Cz–DPP–Cz in F8BT host, respectively. These maximum absorption wavelengths are slightly longer than those found in solution, suggesting the presence of aggregates in the blend films. The steady-state PL spectra of the blends are displayed in Figure 2 and S16, Supporting Information. For both dyes, a small shift toward longer wavelengths is observed as the doping concentration increases. In addition, these spectra are substantially redshifted compared to those measured in solution. This behavior is due to the presence of aggregates in the CBP and F8BT blends and implies that intermolecular interactions slightly affect the photophysical properties of the DPP dyes in the doped films. It is worth noting that the slight increase of the (0,1) band when increasing the doping concentration supports well this statement about the existence of molecular aggregates in the doped films.[67] As shown in Figure 2, S16 and Table S5–S8, Supporting Information, the emission spectra and PLQY values of the CBP and F8BT blends were then measured as a function of the doping concentration. For both dyes, the PLQY is found to gradually increase as the doping concentration decreases. For instance, the PLQY of TPA–DDP–TPA (Cz–DDP–Cz) in CBP increases from 32 (34) to 58 (62)% as the doping concentration decreases from 6 to 1 wt%. Noticeably, the PLQYs of the two DPP derivatives at 1 wt% in the CBP host are closer to the values measured in the solution, indicating that the aggregation-caused concentration quenching of the fluorescence has been substantially reduced in these blend films. We note, however, that the FRET from the host to the dyes is not complete in the two CBP blends since some blue fluorescence from the host can be observed when photoexciting the films in the UV region (at 375 nm in the lowest CBP transition, Figure 2b and S16, Supporting Information). In F8BT, the PLQY of TPA–DPP–TPA has been measured to span from 41.5 to 13.5% for 1 to 6 wt%, respectively, and from 45 to 10.5% for to 6 wt%, for Cz–DPP–Cz. The PLQY values measured in F8BT are thus lower than those determined in CBP and we therefore excluded this host for the device measurements. Overall, these photophysical results indicate that the aggregation-caused concentration quenching of the fluorescence of the DPP dyes in CBP blend films can be significantly reduced by optimizing the doping concentration in the host. This aspect is evidently critical to be able to use these compounds as emitters in high-efficiency OLEDs and organic semiconductor lasers.[68–70]

To characterize the EL properties of the two DPP derivatives, we fabricated OLEDs with the following device architectures: indium tin oxide (ITO) (100 nm)/poly(3,4-ethylenedioxythiophene): poly(styrenesulfonate) (PEDOT:PSS) (45 nm)/EML (≈80 nm)/bis {2-[di(phenyl) phosphino]-phenyl ether oxide (DPEPO) (10 nm)/

© 2025 The Author(s). ChemPhotoChem published by Wiley-VCH GmbH

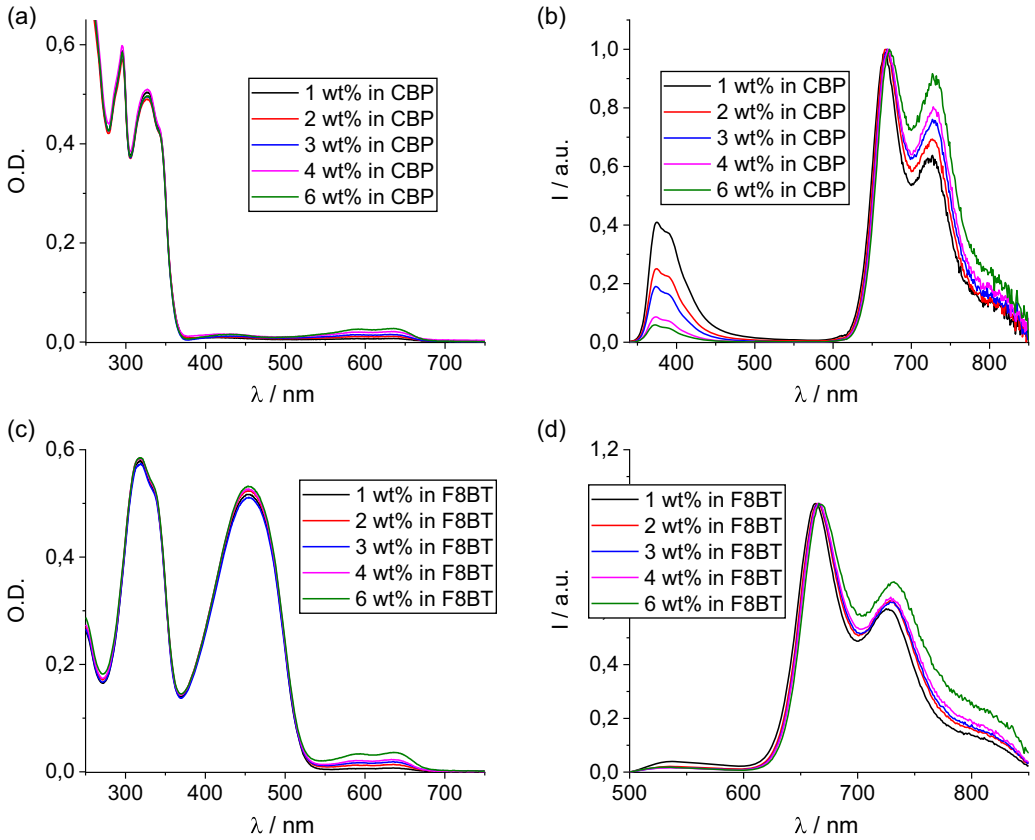


Figure 2. UV/visible electronic absorption and fluorescence emission spectra of a blended films at various dye concentrations of Cz–DPP–Cz in a,b) CBP and c,d) F8BT, respectively.

2,2′,2′-(1,3,5-benzinetriyl)-tris(1-phenyl-1-H-benzimidazole) (TPBi) (55 nm)/LiF (1 nm)/Al (100 nm), where EML corresponds to the emitting layer based on the CBP blends doped with the DPP derivatives at different concentrations (i.e., 1, 2, and 4 wt%). In such multilayer OLED structures, PEDOT:PSS, DPEPO, and TPBi served as hole injection, hole blocking, and electron transport layers, respectively.

An energy-level diagram of these OLEDs is provided in **Figure 3**a. The current density–voltage (*J*–*V*) curves measured for these devices are displayed in Figure S17, Supporting Information, and show that their turn-on voltage slightly varies with the doping concentration. Such a behavior indicates that the excitons are preferentially formed by direct charge trapping on the dopant molecules.[71,72] This statement is well supported by the EL spectra shown in **Figure 4**b,c where no emission from the CBP host can be observed, despite the incomplete energy transfer to the dopant molecules evidenced by the photophysical measurements as illustrated in Figure 4b,c. The EL spectra of the two DPP derivatives are consistent with what was obtained upon photoexcitation and, together with the pictures in the insets of Figure 4b,c, demonstrate that these compounds can be used as emitters in far-red/NIR OLEDs. Figure 4d shows the EQE versus current density (EQE–*J*) characteristics of the OLEDs. As the doping concentration decreases from 4 to 1 wt%, the maximum EQE values increase from 1 to 1.9% for TPA–DPP–TPA and from 1.25 to 2.1% for Cz–DPP–Cz. Such a behavior is in good agreement with the trends observed in the doping concentration dependence of the PLQY of the two emitters. It can also be seen from the EQE–*J* curves that the devices show some efficiency roll-off as the current density increases up to 100 mA cm^{-2}, presumably due to a non-optimized charge balance in the EML.[72] Considering the PLQY values of the CBP blends, the EQE values are lower than the theoretical maximum values that can be calculated for fluorescent OLEDs assuming that the light outcoupling efficiency is 20%. These results suggest that the EL properties of the two DPP derivatives can still be optimized by engineering the OLED architecture in order to reduce the efficiency roll-off and enhance the maximum EQE values. Nevertheless, the EL performances of these fluorescent OLEDs are sufficient in the frame of the present study to demonstrate the potential of these dyes for organic far-red/NIR EL devices.

The ASE properties of TPA–DPP–TPA and Cz–DPP–Cz were investigated using thin excitation stripe technique[53,73–76] in the CBP blend films spin-coated on top of fused silica substrates. This method allows to compare the ASE performance of different light-emitting dyes and their potential for organic semiconductor lasers without the use of any feedback resonator structures. In this experimental technique, the organic thin films are irradiated by a laser stripe and the emission spectra are recorded from the edge of the film. Spontaneous emission propagating in the waveguiding film is amplified because of stimulated emission, which leads to a line narrowing of the emission spectrum above a given ASE threshold. Figure 4a,b shows the emission spectra of two CBP blend films (doped at 1 wt% by TPA–DPP–TPA and Cz–DPP–Cz, respectively) below and above the ASE threshold.

© 2025 The Author(s). ChemPhotoChem published by Wiley-VCH GmbH

23670932, 2025, 7, Downloaded from https://chemistry-europe.onlinelibrary.wiley.com/doi/10.1002/cptc.202500039 by Ewha Womans University Library, Wiley Online Library on [07/12/2025]. See the Terms and Conditions (https://onlinelibrary.wiley.com/terms-and-conditions) on Wiley Online Library for rules of use; OA articles are governed by the applicable Creative Commons License

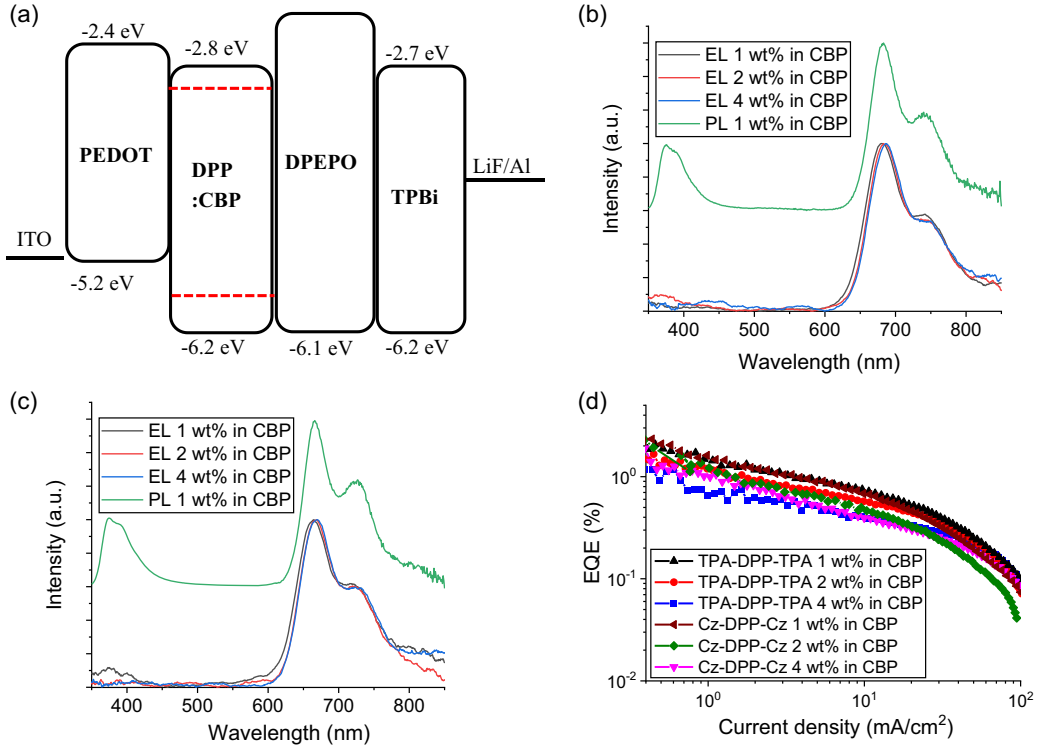


Figure 3. a) Energy-level diagram of the OLED devices; b) EL at different dye concentrations in CBP and photoluminescence (1 wt% in CBP) of TPA–DPP–TPA; c) EL at different dye concentrations in CBP and photoluminescence (1 wt% in CBP) of Cz–DPP–Cz; and d) EQE versus current density of TPA–DPP–TPA and Cz–DPP–Cz blended in CBP.

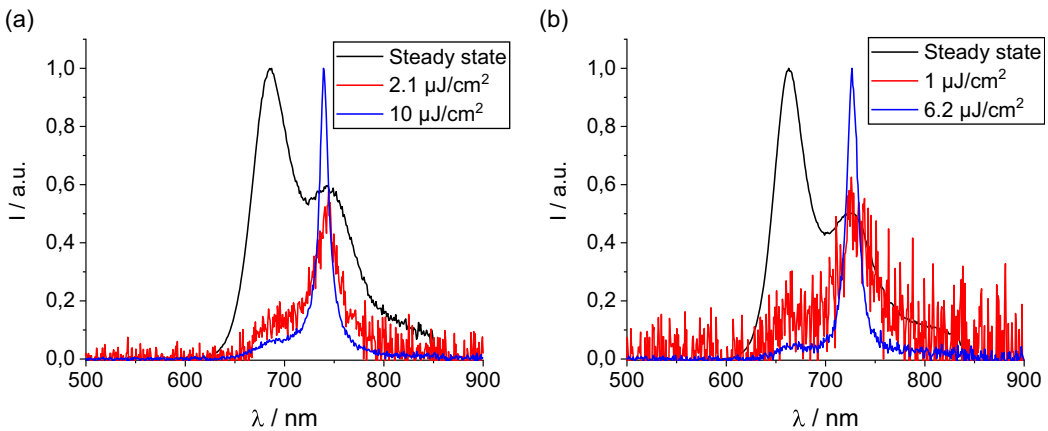


Figure 4. Steady-state emission spectrum (black), spectrum below threshold (red) and above threshold (blue) of CBP blend films (120 nm thick) doped at 1 wt% by a) TPA–DPP–TPA and b) Cz–DPP–Cz.

Since the optical gain is related to the PLQY of the active lasing material,[57] we only examine here the ASE properties of the 1, 2, and 4 wt% CBP blends. Note that for the results shown in Figure 4a,b, film thicknesses of the films containing TPA–DPP–TPA and Cz–DPP–Cz were measured to be around 120 nm. Such a thickness was optimized by measuring the threshold of 1 wt% CBP blends using film of different thicknesses (Figure S18 and S19, Supporting Information) demonstrating the influence of the thickness on the threshold.[77,78] At low excitation densities, it can be seen that the emission spectra from the edge of the film are broad, similar to the steady-state fluorescence spectra and do not change with the pumping intensity. At excitation densities higher than the ASE threshold, spectral narrowing of the emission band is clearly observed for the two dyes (Figure 4). Noticeably, light amplification occurs at 739 and 727 nm for the blends containing 1 wt% TPA–DPP–TPA and Cz–DPP–Cz, respectively. As expected, this line narrowing effect is observed near the (0,1) vibronic transitions of the dyes, which corresponds to the situation of a quasi-four-level vibronic system.

Figure 5a,b displays the output light intensity emitted from the edge of the waveguiding films and the full-width-at-half-maximum (FWHM) of the emission spectra as a function of the

© 2025 The Author(s). ChemPhotoChem published by Wiley-VCH GmbH

23670932, 2025, 7, Downloaded from https://chemistry-europe.onlinelibrary.wiley.com/doi/10.1002/cptc.202500039 by Ewha Womans University Library, Wiley Online Library on [07/12/2025]. See the Terms and Conditions (https://onlinelibrary.wiley.com/terms-and-conditions) on Wiley Online Library for rules of use; OA articles are governed by the applicable Creative Commons License

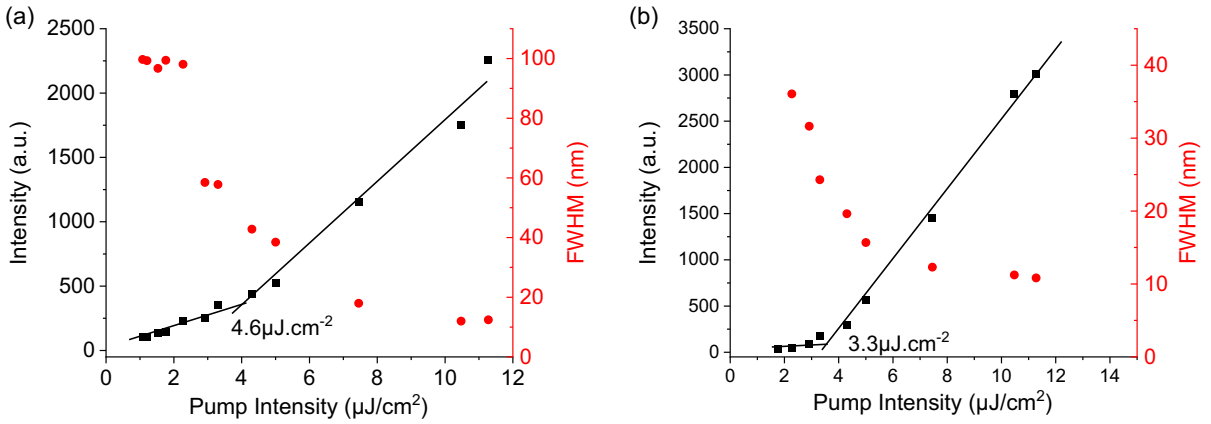


Figure 5. Output intensity emitted from the edge of the films as a function of the pumping intensity and variation of the FWHM with the pumping intensity for a) TPA–DPP–TPA and b) Cz–DPP–Cz in a 1 wt% CBP blend.

excitation density. In both CBP blends, the FWHM is found to collapse from 94 to 11 nm for TPA–DPP–TPA (82 to 10 nm for Cz–DPP–Cz) as the excitation density increases above the ASE threshold. Looking at the evolution of the curves plotting the output light intensity against the excitation density, the changes in slope efficiency are directly related to the ASE thresholds of the two samples. The TPA–DPP–TPA and Cz–DPP–Cz dyes in the 1 wt% CBP blends are found to exhibit an ASE threshold of 4.6 and 3.3 μJ cm^{-2} (Figure S20 and S21, Supporting Information) with a half-life stability of 30 and 65 s, respectively (Figure S22, Supporting Information). For comparison, the most promising NIR D–A–D boron difluoride curcuminoid derivative reported so far shows an ASE threshold of 7 μJ cm^{-2} in a 6 wt% CBP blend. This value is slightly higher than those measured for the two DPP derivatives, providing evidence that these materials are promising candidates for NIR organic semiconductor lasers. Furthermore, benzobis(thiadiazole) derivatives that are surrounded by capped fluorene unit showed NIR ASE (above 800 nm) with a threshold of around 4 μJ cm^{-2} but with inefficient OLED operation (i.e., very low EQE).[79] Finally, we checked the PLQY dependence on the ASE threshold by measuring 2 and 4 wt% blends in CBP and confirmed that the threshold increased with the increased concentration (i.e., when the PLQYs decreased). This study, therefore, demonstrates that DPP derivatives can be ranked among the most promising families of dyes for NIR organic solid-state lasing and are suitable for the realization of high-performance NIR light-emitting devices and applications.

3. Conclusion

In conclusion, we investigated the photophysical, electroluminescent, and ASE properties of two solution-processable far-red/NIR fluorescent DPP derivatives. With PLQY values around 60%, maximum external quantum EL efficiency values as high as 2% and ASE threshold as low as 3.5–4.5 μJ cm^{-2}, the results demonstrate the excellent potential of these compounds for organic light-emitting applications. There are only few organic materials showing in thin films an ASE threshold around or lower than 1 μJ cm^{-2}.[56,79–83] In addition, most of these high-efficiency laser dyes mostly emit in the blue region of the electromagnetic spectrum. In that context, based on this study, we claim that advanced DPP derivatives can be considered high-performance emitters for far-red and NIR organic semiconductor lasers. While these fluorescent emitters also exhibit promising electroluminescent properties, future works should clarify the true potential of these dyes as terminal emitters in far-red/NIR hyperfluorescent OLEDs[84] and for the realization of electrically pumped NIR organic laser diodes.

4. Experimental Section

Materials Synthesis

Details on the synthesis, purification, and characterization of the chemical properties of molecules TPA–DPP–TPA and Cz–DPP–Cz are provided in the Supporting Information section (Figure S1–S4, Supporting Information).

Quantum Chemical Calculations

Ground and first singlet excited states of Cz–DPP–Cz and TPA–DPP–TPA were optimized using the hybrid functional PBE0[85] and the long-range-corrected ωB97X-D functional[86] that incorporates a Grimme's D2 dispersion model in its formulation. The dispersion correction is designed to account for long-range van der Waals interactions. The 6-31G(d,p) basis set[87] was employed in both cases, including polarization corrections for all atoms. All the quantum chemical calculations were performed with the Gaussian 16 suite of programs.[88] The vibronically resolved absorption and emission spectra were simulated within the Franck–Condon approximation considering the VH approach, as implemented in FCClasses 3.3.[59]

Photophysical Measurements

For the characterization of photophysical properties in solution, molecules TPA–DPP–TPA and Cz–DPP–Cz were dissolved in solvents having different polarities at concentrations of ≈10^{-6} M and the solutions were placed in quartz cuvettes. All solvents used for these

© 2025 The Author(s). ChemPhotoChem published by Wiley-VCH GmbH

23670932, 2025, 7, Downloaded from https://chemistry-europe.onlinelibrary.wiley.com/doi/10.1002/cptc.202500039 by Ewha Womans University Library, Wiley Online Library on [07/12/2025]. See the Terms and Conditions (https://onlinelibrary.wiley.com/terms-and-conditions) on Wiley Online Library for rules of use; OA articles are governed by the applicable Creative Commons License

photophysical measurements were of spectroscopic grade. For the characterization of the photophysical and ASE properties in thin films, the films were deposited onto precleaned fused silica substrates by spin coating from chloroform solution. The thicknesses of these films were measured using a Dektak profilometer.

Absorption spectra in both solution and film were recorded using a Varian Cary 5000 spectrometer and a UV-2550 spectrometer (Shimadzu), respectively. Steady-state PL spectra were obtained using a Fluoromax-4 spectrophotometer (Horiba Scientific) and corrected following the procedure reported by Parker et al.[89] to take into account the response of the detector.[90] The PLQY values were measured using an integrating sphere system coupled with a photonic multichannel analyzer (Hamamatsu Photonics C9920-02, PMA-11).

For the time-resolved PL measurements at room temperature, thin films were placed in air. A nitrogen laser (Ken-X, Usho Optical systems) delivering 500 ps excitation pulses with a wavelength of 337 nm and a repetition rate of 20 Hz was used for photoexcitation. The transient PL emission was recorded using a streak camera (Hamamatsu Photonics C4334).

To characterize the ASE properties, the samples in nitrogen atmosphere were photoexcited by a nitrogen laser (excitation wavelength of 337 nm, pulse width of 800 ps and repetition rate of 8 Hz). A set of neutral density filters were used to vary the energy of the excitation pulses. The excitation beam was focused using a cylindrical lens into a stripe of dimension 0.5 cm × 0.08 cm. The emission was detected from the edge of the organic film using an optical fiber connected to a charge-coupled device spectrometer (PMA-11, Hamamatsu Photonics).

Electrochemistry

Cyclic voltammetric data were acquired using a BAS 100 Potentiostat (Bioanalytical Systems) and a PC computer containing BAS100W software (v2.3). A three-electrode system with a Pt working electrode (diameter 1.6 mm), a Pt counter electrode, and an Ag/AgCl (with 3M NaCl filling solution) reference electrode was used. $[(^nBu)_4N]PF_6$ (0.1 M in CH_2Cl_2) served as an inert electrolyte. Cyclic voltammograms were recorded at a scan rate of 100 mV s^{-1}. Ferrocene was used as the internal standard (+0.46 V vs SCE).[91]

Device Fabrication and Measurements

For the fabrication of OLEDs, poly(3,4-ethylenedioxythiophene): poly(styrenesulfonate) (PEDOT:PSS) was purchased from Heraeus Clevios while 4,4′-bis(*N*-carbazolyl)-1,10-biphenyl (CBP), 2,2′,2″-(1,3,5-benzinetriyl)-tris(1-phenyl-1-H-benzimidazole) (TPBi) and bis{2-[di(phenyl)phosphino]-phenyl ether oxide (DPEPO) were supplied by TCI chemicals. The PEDOT:PSS layers were spin-coated on top of cleaned prepatterned ITO glass substrates and then annealed at 180 °C for 30 min. Blends with different doping concentrations were spin-coated on top of the PEDOT:PSS layer from a chloroform solution. DPEPO and TPBi films were then thermally evaporated and cathodes consisting of 1 nm thick LiF and 100 nm thick Al were finally deposited by thermal evaporation to complete the devices. The active area of the devices was designed to be 4 mm^2. Importantly, the devices were encapsulated in a glove box filled with nitrogen to avoid contamination by oxygen and moisture. For OLED characterization, current (*J*)–voltage (*V*)–luminance (*L*) characteristics were obtained under direct current (DC) driving using a source meter (Keithley 2400, Keithley Instruments Inc.) and EQE measurements were performed using a C9920-12 Hamamatsu Photonics detector. The EL spectra were recorded using an optical fiber connected to a spectrometer (PMA-12, Hamamatsu Photonics).

Acknowledgements

This work was supported by the Agence Nationale de la Recherche through the project Despot-Dyes (ANR-23-CE30-0003), through the framework of the French Investments for the Future Program Idex, UNISTRA (ANR-10-IDEX-0002) and SFRI STRAT'US project (ANR-20-SFRI-0012), financing the Interdisciplinary Thematic Institute HiFunMat (part of the ITI 2021-2028 of the UNISTRA, CNRS, and INSERM UMR 1121) and by Institut Carnot MICA. J.-C.R. thanks the Engineering and Physics Sciences Research Council of the UK for financial support from grant EP/Y021495/1. The authors also acknowledge JST CREST (grant no. JPMJCR22B3) and JSPS KAKENHI International Leading Research (ILR) (grant no. 23K20039). The authors want to acknowledge Arnaud Marquette and Damien Cianfarani (OPTIC′ characterization facility of IPCMS) and Emilie Couzigné, Marie-Noëlle Lalloz-Vogel, Nicolas Beyer, for the quality of their work and their willingness all along this project. Y.O., D.V., and M.F. acknowledge funding by the Fonds de la Recherche Scientifique-FNRS under grant no. T.0226.24 (OMLED). Computational resources were also provided by the "Consortium des Équipements de Calcul Intensif" (CÉCI), funded by the "Fonds de la Recherche Scientifiques de Belgique" (FRS-FNRS) under grant no. 2.5020.11.

Conflict of Interest

The authors declare no conflict of interest.

Author Contributions

Anthony D'Aléo: conceptualization (lead); formal analysis (lead); supervision (lead); validation (lead); writing—original draft (lead); writing—review and editing (lead). **Virginie Placide**: conceptualization (lead); formal analysis (lead); investigation (lead); writing—review and editing (equal). **Hao Ye**: conceptualization (equal); investigation (equal); writing—review and editing (supporting). **Matteo Fornasarig**: investigation (equal). **Danillo Valverde**: formal analysis (equal); investigation (equal); writing—review and editing (supporting). **Eunyoung Choi**: investigation (equal). **Gabriel Canard**: formal analysis (equal); investigation (equal); writing—original draft (equal); writing—review and editing (equal). **Jeong Weon Wu**: funding acquisition (equal); investigation (equal). **Yoann Olivier**: formal analysis (lead); investigation (lead); supervision (lead); writing—original draft (lead); writing—review and editing (lead). **Chihaya Adachi**: formal analysis (equal); funding acquisition (equal); supervision (lead); writing—review and editing (equal). **Jean-Charles Ribierre**: conceptualization (equal); investigation (equal); supervision (lead); writing—original draft (lead); writing—review and editing (lead).

Data Availability Statement

The data that support the findings of this study are available from the corresponding author upon reasonable request.

© 2025 The Author(s). ChemPhotoChem published by Wiley-VCH GmbH

23670932, 2025, 7, Downloaded from https://chemistry-europe.onlinelibrary.wiley.com/doi/10.1002/cptc.202500039 by Ewha Womans University Library, Wiley Online Library on [07/12/2025]. See the Terms and Conditions (https://onlinelibrary.wiley.com/terms-and-conditions) on Wiley Online Library for rules of use; OA articles are governed by the applicable Creative Commons License

Keywords: diketopyrrolopyrrole derivatives · fluorescent near-infrared laser dyes · low amplified spontaneous emission threshold · near-infrared organic light-emitting diodes · organic semiconductor lasers

[1] L. Zhu, M. Zhang, J. Xu, C. Li, J. Yan, G. Zhou, W. Zhong, T. Hao, J. Song, X. Xue, Z. Zhou, R. Zeng, H. Zhu, C.-C. Chen, R. C. I. MacKenzie, Y. Zou, J. Nelson, Y. Zhang, Y. Sun, F. Liu, *Nat. Mater.* **2022**, *21*, 656.
[2] J. Peet, J. Y. Kim, N. E. Coates, W. L. Ma, D. Moses, A. J. Heeger, G. C. Bazan, *Nat. Mater.* **2007**, *6*, 497.
[3] T. Xu, L. Yu, *Mater. Today* **2014**, *17*, 11.
[4] G. Li, W.-H. Chang, Y. Yang, *Nat. Rev. Mater.* **2017**, *2*, 17043.
[5] J. C. Ribierre, M. Sato, A. Ishizuka, T. Tanaka, S. Watanabe, M. Matsumoto, S. Matsumoto, M. Uchiyama, T. Aoyama, *Org. Electron.* **2012**, *13*, 999.
[6] M. C. Scharber, N. S. Sariciftci, *Adv. Mater. Tech.* **2021**, *6*, 2000857.
[7] E. J. Meijer, D. M. De Leeuw, S. Setayesh, E. Van Veenendaal, B.-H. Huisman, P. W. M. Blom, J. C. Hummelen, U. Scherf, T. M. Klapwijk, *Nat. Mater.* **2003**, *2*, 678.
[8] M. Zhang, H. N. Tsao, W. Pisula, C. Yang, A. K. Mishra, K. Müllen, *J. Am. Chem. Soc.* **2007**, *129*, 3472.
[9] J.-C. Ribierre, T. Tanaka, L. Zhao, Y. Yokota, S. Matsumoto, D. Hashizume, K. Takaishi, T. Muto, B. Heinrich, S. Méry, F. Mathevet, T. Matsushima, M. Uchiyama, C. Adachi, T. Aoyama, *Adv. Funct. Mater.* **2018**, *28*, 1707038.
[10] S. Tasch, E. J. W. List, C. Hochfilzer, G. Leising, P. Schlichting, U. Rohr, Y. Geerts, U. Scherf, K. Müllen, *Phys. Rev. B* **1997**, *56*, 4479.
[11] O. Fenwick, J. K. Sprafke, J. Binas, D. V. Kondratuk, F. Di Stasio, H. L. Anderson, F. Cacialli, *Nano Lett.* **2011**, *11*, 2451.
[12] A. D'Aléo, M. H. Sazzad, D. H. Kim, E. Y. Choi, J. W. Wu, G. Canard, F. Fages, J.-C. Ribierre, C. Adachi, *Chem. Commun.* **2017**, *53*, 7003.
[13] Y. Zhang, Y. Wang, J. Song, J. Qu, B. Li, W. Zhu, W.-Y. Wong, *Adv. Opt. Mater.* **2018**, *6*, 1800466.
[14] H. F. Higginbotham, P. Pander, R. Rybakiewicz, M. K. Etherington, S. Maniam, M. Zagorska, A. Pron, A. P. Monkman, P. Data, *J. Mater. Chem. C* **2018**, *6*, 8219.
[15] L. Yao, S. Zhang, R. Wang, W. Li, F. Shen, B. Yang, Y. Ma, *Angew. Chem. Int. Ed.* **2014**, *53*, 2119.
[16] G. Qian, Z. Zhong, M. Luo, D. Yu, Z. Zhang, Z. Y. Wang, D. Ma, *Adv. Mater.* **2009**, *21*, 111.
[17] P. Murto, A. Minotto, A. Zampetti, X. Xu, M. R. Andersson, F. Cacialli, E. Wang, *Adv. Opt. Mater.* **2016**, *4*, 2068.
[18] R. Yang, R. Tian, J. Yan, Y. Zhang, J. Yang, Q. Hou, W. Yang, C. Zhang, Y. Cao, *Macromolecules* **2005**, *38*, 244.
[19] S. Gao, Z. Cui, F. Li, *Chem. Soc. Rev.* **2023**, *52*, 2875.
[20] K. R. Graham, Y. Yang, J. R. Sommer, A. H. Shelton, K. S. Schanze, J. Xue, J. R. Reynolds, *Chem. Mater.* **2011**, *23*, 5305.
[21] L. Huang, C. D. Park, T. Fleetham, J. Li, *Appl. Phys. Lett.* **2016**, *109*, 233302.
[22] P. L. Dos Santos, P. Stachelek, Y. Takeda, P. Pander, *Mater. Chem. Front.* **2024**, *8*, 1731.
[23] A. Shahalizad, A. D'Aléo, C. Andraud, M. H. Sazzad, D.-H. Kim, Y. Tsuchiya, J.-C. Ribierre, J.-M. Nunzi, C. Adachi, *Org. Electron.* **2017**, *44*, 50.
[24] L. H. Slooff, A. Polman, F. Cacialli, R. H. Friend, G. A. Hebbink, F. C. J. M. Van Veggel, D. N. Reinhoudt, *Appl. Phys. Lett.* **2001**, *78*, 2122.
[25] J. V. Caspar, E. M. Kober, B. P. Sullivan, T. J. Meyer, *J. Am. Chem. Soc.* **1982**, *104*, 630.
[26] K. Tuong Ly, R.-W. Chen-Cheng, H.-W. Lin, Y.-J. Shiau, S.-H. Liu, P.-T. Chou, C.-S. Tsao, Y.-C. Huang, Y. Chi, *Nat. Photon.* **2017**, *11*, 63.
[27] S.-F. Wang, B.-K. Su, X.-Q. Wang, Y.-C. Wei, K.-H. Kuo, C.-H. Wang, S.-H. Liu, L.-S. Liao, W.-Y. Hung, L.-W. Fu, W.-T. Chuang, M. Qin, X. Lu, C. You, Y. Chi, P.-T. Chou, *Nat. Photon.* **2022**, *16*, 843.
[28] Y.-C. Wei, K.-H. Kuo, Y. Chi, P.-T. Chou, *Acc. Chem. Res.* **2023**, *56*, 689.
[29] S. Wang, D. Zhou, K. Kuo, C. Wang, C. Hung, J. Yan, L. Liao, W. Hung, Y. Chi, P. Chou, *Angew. Chem. Int. Ed.* **2024**, *63*, e202317571.
[30] A. Endo, M. Ogasawara, A. Takahashi, D. Yokoyama, Y. Kato, C. Adachi, *Adv. Mater.* **2009**, *21*, 4802.
[31] D.-H. Kim, A. D'Aléo, X.-K. Chen, A. D. S. Sandanayaka, D. Yao, L. Zhao, T. Komino, E. Zaborova, G. Canard, Y. Tsuchiya, E. Choi, J. W. Wu, F. Fages, J.-L. Brédas, J.-C. Ribierre, C. Adachi, *Nat. Photon.* **2018**, *12*, 98.
[32] H. Ye, D. H. Kim, X. Chen, A. S. D. Sandanayaka, J. U. Kim, E. Zaborova, G. Canard, Y. Tsuchiya, E. Y. Choi, J. W. Wu, F. Fages, J.-L. Bredas, A. D'Aléo, J.-C. Ribierre, C. Adachi, *Chem. Mater.* **2018**, *30*, 6702.
[33] T. Yamanaka, H. Nakanotani, S. Hara, T. Hirohata, C. Adachi, *Appl. Phys. Express* **2017**, *10*, 074101.
[34] Y. Yuan, Y. Hu, Y.-X. Zhang, J.-D. Lin, Y.-K. Wang, Z.-Q. Jiang, L.-S. Liao, S.-T. Over Lee, *Adv. Funct. Mater.* **2017**, *27*, 1700986.
[35] T. Hua, N. Li, Z. Huang, Y. Zhang, L. Wang, Z. Chen, J. Miao, X. Cao, X. Wang, C. Yang, *Angew. Chem. Int. Ed.* **2024**, *63*, e202318433.
[36] Z. Hao, A. Iqbal, *Chem. Soc. Rev.* **1997**, *26*, 203.
[37] K. Zhang, B. Tieke, *Macromolecules* **2008**, *41*, 7287.
[38] S. Stas, J.-Y. Balandier, V. Lemaur, O. Fenwick, G. Tregnago, F. Quist, F. Cacialli, J. Cornil, Y. H. Geerts, *Dyes Pigm.* **2013**, *97*, 198.
[39] S. Qu, W. Wu, J. Hua, C. Kong, Y. Long, H. Tian, *J. Phys. Chem. C* **2010**, *114*, 1343.
[40] W. Li, K. H. Hendriks, M. M. Wienk, R. A. J. Janssen, *Acc. Chem. Res.* **2016**, *49*, 78.
[41] M. Shahid, R. S. Ashraf, Z. Huang, A. J. Kronemeijer, T. McCarthy-Ward, I. McCulloch, J. R. Durrant, H. Sirringhaus, M. Heeney, *J. Mater. Chem.* **2012**, *22*, 12817.
[42] C. B. Nielsen, M. Turbiez, I. McCulloch, *Adv. Mater.* **2013**, *25*, 1859.
[43] M. M. Wienk, M. Turbiez, J. Gilot, R. A. J. Janssen, *Adv. Mater.* **2008**, *20*, 2556.
[44] J. C. Bijleveld, A. P. Zoombelt, S. G. J. Mathijssen, M. M. Wienk, M. Turbiez, D. M. de Leeuw, R. A. J. Janssen, *J. Am. Chem. Soc.* **2009**, *131*, 16616.
[45] M. Sassi, N. Buccheri, M. Rooney, C. Botta, F. Bruni, U. Giovanella, S. Brovelli, L. Beverina, *Sci. Rep.* **2016**, *6*, 34096.
[46] M. Fukuda, K. Kodama, H. Yamamoto, K. Mito, *Dyes Pigm.* **2004**, *63*, 115.
[47] S. Mula, D. Hablot, K. K. Jagtap, E. Heyer, R. Ziessel, *New J. Chem.* **2013**, *37*, 303.
[48] J. S. Zambounis, Z. Hao, A. Iqbal, *Nature* **1997**, *388*, 131.
[49] S. S. Bagde, H. Park, S. Yang, S.-H. Jin, S.-H. Lee, *Chem. Phys. Lett.* **2015**, *630*, 37.
[50] O. P. Lee, A. T. Yiu, P. M. Beaujuge, C. H. Woo, T. W. Holcombe, J. E. Millstone, J. D. Douglas, M. S. Chen, J. M. J. Fréchet, *Adv. Mater.* **2011**, *23*, 5359.
[51] Z. Cai, Z. Liu, X. Wu, J. Guo, B. Z. Tang, Z. Zhao, *Adv. Opt. Mater.* **2023**, *11*, 2300404.
[52] Y. Li, L. Li, Y. Wu, Y. Li, *J. Phys. Chem. C* **2017**, *121*, 8579.
[53] I. D. W. Samuel, G. A. Turnbull, *Chem. Rev.* **2007**, *107*, 1272.
[54] T. Aimono, Y. Kawamura, K. Goushi, H. Yamamoto, H. Sasabe, C. Adachi, *Appl. Phys. Lett.* **2005**, *86*, 071110.
[55] A. S. D. Sandanayaka, T. Matsushima, F. Bencheikh, K. Yoshida, M. Inoue, T. Fujihara, K. Goushi, J.-C. Ribierre, C. Adachi, *Sci. Adv.* **2017**, *3*, e1602570.
[56] D.-H. Kim, A. S. D. Sandanayaka, L. Zhao, D. Pitrat, J. C. Mulatier, T. Matsushima, C. Andraud, J. C. Ribierre, C. Adachi, *Appl. Phys. Lett.* **2017**, *110*, 023303.
[57] J. C. Ribierre, G. Tsiminis, S. Richardson, G. A. Turnbull, I. D. W. Samuel, H. S. Barcena, P. L. Burn, *Appl. Phys. Lett.* **2007**, *91*, 081108.
[58] E. Y. Choi, L. Mazur, L. Mager, M. Gwon, D. Pitrat, J. C. Mulatier, C. Monnereau, A. Fort, A. J. Attias, K. Dorkenoo, J. E. Kwon, Y. Xiao, K. Matczyszyn, M. Samoc, D.-W. Kim, A. Nakao, B. Heinrich, D. Hashizume, M. Uchiyama, S. Y. Park, F. Mathevet, T. Aoyama, C. Andraud, J. W. Wu, A. Barsella, J. C. Ribierre, *Phys. Chem. Chem. Phys.* **2014**, *16*, 16941.
[59] J. Cerezo, F. Santoro, *J. Comput. Chem.* **2023**, *44*, 626.
[60] A. Dreuw, M. Head-Gordon, *Chem. Rev.* **2005**, *105*, 4009.
[61] J. Cerezo, D. Aranda, F. J. Avila Ferrer, G. Prampolini, F. Santoro, *J. Chem. Theory Comput.* **2020**, *16*, 1215.
[62] J. Cerezo, L. Martínez-Fernández, R. Improta, F. Santoro, *Theor. Chem. Acc.* **2016**, *135*, 221.
[63] T. J. Zuehlsdorff, C. M. Isborn, *Int. J. Quantum Chem.* **2019**, *119*, e25719.
[64] T.H. Förster, *Ann. Phys.* **1948**, *437*, 55.
[65] A. Ruseckas, J. C. Ribierre, P. E. Shaw, S. V. Staton, P. L. Burn, I. D. W. Samuel, *Appl. Phys. Lett.* **2009**, *95*, 183305.
[66] K. J. Lee, J. H. Woo, E. Kim, Y. Xiao, X. Su, L. M. Mazur, A.-J. Attias, F. Fages, O. Cregut, A. Barsella, F. Mathevet, L. Mager, J. W. Wu, A. D'Aléo, J.-C. Ribierre, *Phys. Chem. Chem. Phys.* **2016**, *18*, 7875.
[67] F. C. Spano, *Acc. Chem. Res.* **2010**, *43*, 429.
[68] E. B. Namdas, A. Ruseckas, I. D. W. Samuel, S.-C. Lo, P. L. Burn, *J. Phys. Chem. B* **2004**, *108*, 1570.
[69] Y. Kawamura, J. Brooks, J. J. Brown, H. Sasabe, C. Adachi, *Phys. Rev. Lett.* **2006**, *96*, 017404.
[70] J. C. Ribierre, A. Ruseckas, K. Knights, S. V. Staton, N. Cumpstey, P. L. Burn, I. D. W. Samuel, *Phys. Rev. Lett.* **2008**, *100*, 017402.
[71] E. Gautier-Thianche, C. Sentein, A. Lorin, C. Denis, P. Raimond, J.-M. Nunzi, *J. Appl. Phys.* **1998**, *83*, 4236.

© 2025 The Author(s). ChemPhotoChem published by Wiley-VCH GmbH

23670932, 2025, 7, Downloaded from https://chemistry-europe.onlinelibrary.wiley.com/doi/10.1002/cptc.202500039 by Ewha Womans University Library, Wiley Online Library on [07/12/2025]. See the Terms and Conditions (https://onlinelibrary.wiley.com/terms-and-conditions) on Wiley Online Library for rules of use; OA articles are governed by the applicable Creative Commons License

23670932, 2025, 7, Downloaded from https://chemistry-europe.onlinelibrary.wiley.com/doi/10.1002/cptc.202500039 by Ewha Womans University Library, Wiley Online Library on [07/12/2025]. See the Terms and Conditions (https://onlinelibrary.wiley.com/terms-and-conditions) on Wiley Online Library for rules of use; OA articles are governed by the applicable Creative Commons License

[72] L. Zhao, T. Komino, M. Inoue, J.-H. Kim, J. C. Ribierre, C. Adachi, *Appl. Phys. Lett.* **2015**, *106*, 063301.
[73] M. D. McGehee, A. J. Heeger, *Adv. Mater.* **2000**, *12*, 1655.
[74] G. Heliotis, S. A. Choulis, G. Itskos, R. Xia, R. Murray, P. N. Stavrinou, D. D. C. Bradley, *Appl. Phys. Lett.* **2006**, *88*, 081104.
[75] G. Kreiza, P. Baronas, E. Radiunas, P. Adomėnas, O. Adomėnienė, K. Kazlauskas, J.-C. Ribierre, C. Adachi, S. Juršėnas, *Adv. Opt. Mater.* **2017**, *5*, 1600823.
[76] A. J. C. Kuehne, M. C. Gather, *Chem. Rev.* **2016**, *116*, 12823.
[77] G. Heliotis, R. Xia, D. D. C. Bradley, G. A. Turnbull, I. D. W. Samuel, P. Andrew, W. L. Barnes, *J. Appl. Phys.* **2004**, *96*, 6959.
[78] M. G. Ramirez, P. G. Boj, V. Navarro-Fuster, I. Vragovic, J. M. Villalvilla, I. Alonso, V. Trabadelo, S. Merino, M. A. Díaz-García, *Opt. Express* **2011**, *19*, 22443.
[79] X. Tang, Y.-T. Lee, Z. Feng, S. Y. Ko, J. W. Wu, V. Placide, J.-C. Ribierre, A. D'Aléo, C. Adachi, *ACS Mater. Lett.* **2020**, *2*, 1567.
[80] J.-H. Kim, M. Inoue, L. Zhao, T. Komino, S. Seo, J.-C. Ribierre, C. Adachi, *Appl. Phys. Lett.* **2015**, *106*, 053302.
[81] C. Karnutsch, C. Pflumm, G. Heliotis, J. C. deMello, D. D. C. Bradley, J. Wang, T. Weimann, V. Haug, C. Gärtner, U. Lemmer, *Appl. Phys. Lett.* **2007**, *90*, 131104.
[82] H. Nakanotani, S. Akiyama, D. Ohnishi, M. Moriwake, M. Yahiro, T. Yoshihara, S. Tobita, C. Adachi, *Adv. Funct. Mater.* **2007**, *17*, 2328.
[83] H. Nakanotani, C. Adachi, S. Watanabe, R. Katoh, *Appl. Phys. Lett.* **2007**, *90*, 231109.
[84] H. Nakanotani, T. Higuchi, T. Furukawa, K. Masui, K. Morimoto, M. Numata, H. Tanaka, Y. Sagara, T. Yasuda, C. Adachi, *Nat. Commun.* **2014**, *5*, 4016.
[85] C. Adamo, V. Barone, *J. Chem. Phys.* **1999**, *110*, 6158.
[86] J.-D. Chai, M. Head-Gordon, *Phys. Chem. Chem. Phys.* **2008**, *10*, 6615.
[87] R. Ditchfield, W. J. Hehre, J. A. Pople, *J. Chem. Phys.* **1971**, *54*, 724.
[88] M. J. Frisch, G. W. Trucks, H. B. Schlegel, G. E. Scuseria, M. A. Robb, J. R. Cheeseman, G. Scalmani, V. Barone, G. A. Petersson, H. Nakatsuji, X. Li, M. Caricato, A. V. Marenich, J. Bloino, B. G. Janesko, R. Gomperts, B. Mennucci, H. P. Hratchian, J. V. Ortiz, A. F. Izmaylov, J. L. Sonnenberg, F. F. Williams Ding, F. Lipparini, F. Egidi, J. Goings, B. Peng, A. Petrone, T. Henderson, D. Ranasinghe, V. G. Zakrzewski Jr., et al., *Gaussian 16 Rev. C.01* **2016**.
[89] C. A. Parker, *Photoluminescence of Solutions: With Applications to Photochemistry And Analytical Chemistry*, Elsevier, Amsterdam, New York **1969**.
[90] J. R. Lakowicz, *Principles of Fluorescence Spectroscopy*, Springer US, Boston, MA **1999**.
[91] N. G. Connelly, W. E. Geiger, *Chem. Rev.* **1996**, *96*, 877.

Manuscript received: February 5, 2025
Revised manuscript received: March 26, 2025
Version of record online: May 1, 2025

© 2025 The Author(s). ChemPhotoChem published by Wiley-VCH GmbH